Please cite this article in press as: Kwon et al., Efficient calculation of the free energy for protein partitioning using restraining potentials, Biophysical Journal (2023), https://doi.org/10.1016/j.bpj.2022.07.031

Biophysical *Journal*
Article

Biophysical Society

Efficient calculation of the free energy for protein partitioning using restraining potentials

Seulki Kwon,[1] George A. Pantelopulos,[1,2] and John E. Straub[1,*]
[1]Department of Chemistry, Boston University, Boston, Massachusetts and [2]Laboratory of Chemical Physics, National Institute of Diabetes and Digestive and Kidney Diseases, National Institutes of Health, Bethesda, Maryland

ABSTRACT An approach for the efficient simulation of phase-separated lipid bilayers, for use in the calculation of equilibrium free energies of partitioning between lipid domains, is proposed. The methodology exploits restraint potentials and rectangular aspect ratios that enforce lipid phase separation, allowing for the simulation of smaller systems that approximately reproduce bulk behavior. The utility of this approach is demonstrated through the calculation of potentials of mean force for the translation of a transmembrane protein between lipid domains. The impact of the imposed restraints on lipid tail ordering and lipid packing are explored, providing insight into how restraints can best be employed to compute accurate free-energy surfaces. This approach should be useful in the accurate calculation of equilibrium partition coefficients for transmembrane protein partitioning in heterogeneous membranes, providing insight into the thermodynamic driving forces that control this fundamental biophysical phenomenon.

SIGNIFICANCE Lateral heterogeneity in lipid membranes has been proposed to play important functional roles in the cell through the preferential partitioning of proteins that enhances complex formation, enzymatic activity, and signaling. However, little is currently known regarding the thermodynamics of preferential partitioning of proteins between membrane domains. Simulation of phase-separated states is challenging due to the large system sizes required. We present a computational method for efficiently simulating phase-separated systems of smaller size by exploiting both the system aspect ratio and restraining potentials that stabilize the phase-separated state. The accuracy and efficiency of the method are established through the calculation of the free-energy landscape for partitioning of a transmembrane protein between liquid-ordered and -disordered domains.

INTRODUCTION

Lipid membranes composed of a mixture of saturated lipids, unsaturated lipids, and cholesterol may display lateral heterogeneity characterized by the presence of the liquid-disordered (L_d) and the liquid-ordered (L_o) domains (1,2). Tightly packed L_o domains, enriched by cholesterol and saturated lipids and commonly referred to as lipid rafts, are believed to play a critical role in membrane function. They are conjectured to preferentially recruit, colocalize, and thereby promote the formation of functional complexes necessary for transmembrane signaling and protein trafficking (3–5). A protein's affinity for raft domains has been proposed to depend on a variety of features of the protein's transmembrane (TM) domain, including palmitoylation (6,7), hydrophobic length (8,9) informing hydrophobic match and mismatch, and surface area (9). Despite considerable study, our understanding of the thermodynamic driving forces directing protein partitioning into membrane domains remains incomplete.

Fluorescent imaging experiments have been used to assess the preference for protein partitioning into ordered raft domains or disordered fluidic domains (9–11). Surprisingly, a number of proteins previously believed to preferentially partition into L_o domains appear to prefer L_d domains in model membrane systems such as giant unilamellar vesicles (GUVs) or giant plasma membrane vesicles (12,13). In addition, simulation studies have observed that proteins preferentially partition to the domain boundary rather than bulk L_d or L_o domains (6,14,15). Taken together, these observations demonstrate that the factors governing protein partitioning into membrane domains remain poorly understood. Further experimental and computational studies are needed to elucidate this fundamental biophysical phenomenon.

Calculation of the potential of mean force (PMF), assessing the free energy of translating TM proteins between membrane domains, can provide insight into the thermodynamic

Submitted May 31, 2022, and accepted for publication July 25, 2022.
*Correspondence: straub@bu.edu
Editor: Ilya Levental.
https://doi.org/10.1016/j.bpj.2022.07.031

Please cite this article in press as: Kwon et al., Efficient calculation of the free energy for protein partitioning using restraining potentials, Biophysical Journal (2023), https://doi.org/10.1016/j.bpj.2022.07.031

driving forces responsible for protein partitioning. To do this, ternary lipid mixtures comprised of a saturated lipid, an unsaturated lipid, and cholesterol are frequently introduced as they can exhibit the coexistence of different membrane domains (16). The coexistence of the L_d and L_o domains is observed in ternary lipid mixtures at intermediate cholesterol concentrations (10–40 mol %) (17). In addition to lipid composition, the stability of the phase-separated state of a lipid bilayer in molecular dynamics (MD) simulations has been demonstrated to depend on the system size (18–20). To stabilize a phase-separated state, the enthalpic stabilization resulting from lipid partitioning must compensate for the loss of entropy and the cost in free energy of forming the interface (21).

The relative ratio of the interface to bulk also impacts the affinity of proteins for the L_o-L_d domain interface (14). Simulations of liquid mixtures and liquid-vapor interfaces have introduced an anisotropy to the dimensions used in the periodic boundary condition to stabilize the phase-separated state. Lengthening one side of the system creates a principal axis for phase separation, enhancing the proportion of a stabilizing bulk to a destabilizing interface. This approach is referred to as the "slab" method (22–25). The introduction of this anisotropy in the *xy* plane of lipid membranes enhances the bulk area without lengthening the interface, thereby stabilizing the phase-separated states.

There are several challenges that we must face in assessing the free energy of partitioning a protein between membrane domains in simulation studies. Lipids at the domain interface explore different conformations than those observed in bulk domains. Substantial fluctuations of membrane structures cause proteins to adopt different conformations at the domain interface. Due to the challenge of sampling protein conformations in bulk domains as well as at the interface, it has proved challenging to quantitatively assess the thermodynamic driving forces defining protein partitioning using coarse-grained or all-atom MD simulations. Furthermore, in simulation studies employing the slab method, the choice of the system's aspect ratio to facilitate phase separation has been relatively arbitrary and has varied among studies (6,8,12,15). Most significantly, how the membrane structures are affected by changes in the system's aspect ratio has not been thoroughly investigated. Therefore, it is essential to systematically investigate the effect of the system's aspect ratio on membrane structures and the associated changes in free energy of partitioning between domains.

The change in free energy associated with the partitioning of gramicidin A between the DMPC and DLPC lipid bilayer has been assessed by Park et al. in all-atom MD simulations (15). They employed a 2:1 *x*:*y* aspect ratio and a flat-bottom restraint potential. Within these restrained systems, umbrella sampling (US) was used to determine the change in free energy as gramicidin A was translated between the bulk phases of DMPC and DLPC lipids. While this approach is effective, it is unclear how the use of an anisotropic aspect ratio in the *xy* plane and a restraint potential along the *x* axis to enforce phase separation impacts the resulting free-energy surface. DMPC and DLPC only differ in their hydrophobic tail length and are expected to have less frustration in membrane structure at the interface. However, the L_d-L_o phase-separated bilayer has substantial fluctuations in membrane structures near the domain interface. Therefore, there is a need to investigate the impact of changing the *xy* plane aspect ratio and flat-bottom restraint potential on the structure of the lipid bilayer and the resulting PMF.

We present an efficient and effective means of modeling phase-separated states of ternary component lipid membranes across different length scales. We modulate the fluctuations in membrane structure at the interface by systematically tuning the system's aspect ratio. In addition, we show that better sampling of the PMF for the translation of protein between domains can be achieved by including a flat-bottom restraint enforcing the interface and reducing the extent of fluctuations. We explore how interfacial fluctuations affect the free-energy landscape for partitioning TM proteins between domains and across domain interfaces. The dependence of interfacial fluctuations on system sizes is characterized in terms of macroscopic line tension and local fluctuations within the length scales of proteins. We demonstrate limitations in the use of the capillary wave theory (7,14,26–28) for describing interfacial line tension when the theory is extended to smaller system sizes. The impact of the system's aspect ratio and imposed lipid restraint on line tension and free energy of protein partitioning is systematically investigated. The proper choice of the system size and aspect ratio, as well as the use of restraints, allow for the efficient and accurate calculations of the free energy of partitioning protein between domains of phase-separated membranes.

MATERIALS AND METHODS

MD simulation

A ternary mixture composed of saturated lipids, unsaturated lipids, and cholesterols was used to investigate the phase-separated lipid bilayer. The MARTINI2.2 force field (29,30) was used to simulate coarse-grained lipid bilayers containing a TM protein using the GROMACS 2018.3 package (31,32). The initial bilayer configuration was built from the lipid mixtures of di-C 16:0 PC (1,2-di-palmitoyl-sn-glycero-3-phosphocholine [DPPC]), di-C 18:2/18:2 PC (1,2-dilinoleoyl-sn-glycero-3-phosphocholine [DIPC]), and cholesterol (CHOL) at 40:40:20 mol % with the *insane.py* script (33).

We chose the smallest system size to be $L_x = 22.4$, $L_y = 11.2$ nm (900 lipids) as this system size is comfortably above the critical system size (see Fig. S1) needed to establish stable phase-separated states in $L_x = L_y$ systems. In addition, this choice determines the interface orientation, as the interface forms parallel to the *y* axis to minimize the length of the interface and free-energy cost of forming the interface. By defining L_x to be longer than L_y, the interface forms parallel to the *y* axis to lower the line tension. The system sizes employed range from 900 to 2700 lipids with different

Please cite this article in press as: Kwon et al., Efficient calculation of the free energy for protein partitioning using restraining potentials, Biophysical Journal (2023), https://doi.org/10.1016/j.bpj.2022.07.031

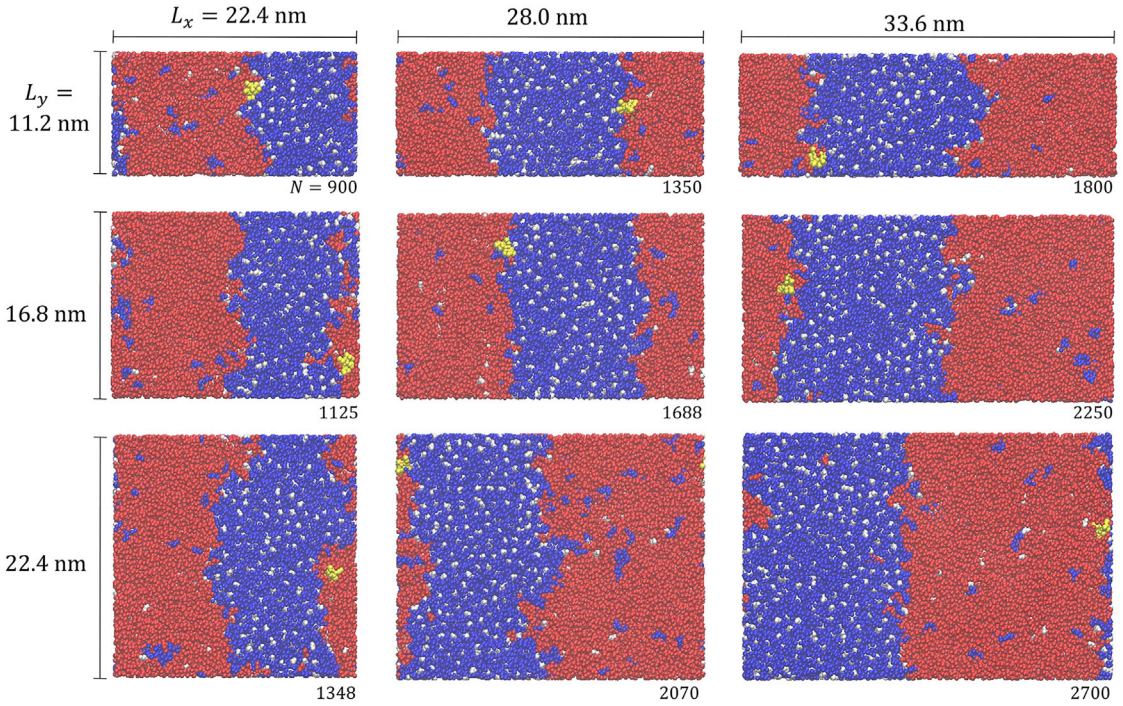

FIGURE 1 Simulation snapshots of different system sizes and aspect ratio investigated in this study. trLAT is colored in yellow, DPPC in blue, DIPC in red, and CHOL in white. L_x and L_y in the figure denote the equilibrium box dimensions along the x and y axis. The total number of lipids (N) is given at the bottom right of the snapshot of each system. To see this figure in color, go online.

lateral sizes L_x and L_y, as shown in Fig. 1. All systems exhibit stable phase separation.

The lipid bilayer was solvated with approximately 12 nonpolarizable MARTINI water particles per lipid. In order to avoid water freezing, 10% of water particles were modeled with antifreeze parameters. A 150 mM salt concentration was used to model physiological conditions. As a model TM protein, the TM domain of the linker for activation of T cells (trLAT) was used. MARTINI parameters for the secondary structure of trLAT were chosen following the previous work of Gorfe and Levental (6). The leap-frog integration method with a 25 fs timestep was used for NPT simulations. A velocity rescaling thermostat was used with 1.0 ps coupling time, and the temperature was set to 295 K (34). A semi-isotropic Berendsen barostat with 2.0 ps coupling time and 3×10^{-4} bar^{-1} compressibility was used (35). Other simulation parameters correspond to the "new-rf" setting described on the MARTINI website (36).

We performed conventional MD simulations with five replicates of each system for 20 μs. The last 4 μs portion of each trajectory was used to analyze the lateral structure and tail ordering of lipids and characterize the L_d/L_o interface. In order to calculate the PMF of trLAT across the L_d-L_o domain interface, US simulations were performed. The reaction coordinate was defined as a distance between the center of mass (COM) of trLAT and the COM of total DIPC lipids. A harmonic bias potential with force constant 1000 kJ mol^{-1} nm^{-2} was used, with umbrella windows separated by 0.2 nm. A 4 μs production run was performed for each umbrella window, following 500 ns of equilibration. The biased probability density obtained from US simulations was unbiased by using the weighted histogram analysis method (37,38).

Imposition of lateral and normal restraint potentials

As the system size and the lateral aspect ratio L_x/L_y increases, the lipid bilayer exhibits larger undulations. The bending of the bilayer at the domain interface substantially distorts the interfacial region. To characterize how the interfacial fluctuations vary with system sizes, we impose a weak harmonic restraint along the z-coordinate positions of a quarter of the DPPC and DIPC molecules in the upper leaflet throughout the simulations to suppress long length scale undulations (see Fig. S2). PO4 beads of randomly chosen lipid molecules were restrained to their average z positions using a harmonic potential with a force constant of 2 kJ mol^{-1} nm^{-2}. This restraint has previously been used for large bilayer systems that exhibit substantial undulations (39,40).

In order to modulate fluctuations of the domain interface, PO4 beads of DPPC and DIPC were restrained using a flat-bottom restraint along the x coordinate (see Fig. 2 *b*). The potential defining this flat-bottom restraint $V(X)$ was

$$V(X) = \frac{1}{2}k_{fb}\left(X - X_{fb}\right)^2 H\left(X - X_{fb}\right), \qquad (1)$$

where X_{fb} is the half width of the flat portion of the potential and k_{fb} is the force constant, which was set to 100 kJ mol^{-1} nm^{-2}. $X = |x_i - x_{ref}|$ is the x distance between the position of the i th lipid x_i and the reference position x_{ref}, defined to be the COM of the L_o region for DPPC or the L_d region for DIPC. To determine X_{fb}, we calculated the average width of the L_o domain ($\overline{X}_{L_o}$) and the L_d domain ($\overline{X}_{L_d}$). X_{fb} was set to $\overline{X}_{L_o}/2 + \Delta$ for DPPC and $\overline{X}_{L_d}/2 + \Delta$ for DIPC, where the additional width $\Delta = 5$ Å was added to avoid additional lateral packing caused by the flat-bottom restraint.

Fig. 2 *a* and *b* show representative snapshots of the lipid bilayer with and without the flat-bottom restraint potential. Fig. 2 *d* shows that interfacial fluctuation of the lipid bilayer in the presence of the flat-bottom restraint potential is greatly reduced compared with the bilayer in the absence of the potential. Fig. 2 *e* and *f* show the time evolution of a given interfacial line for 1 μs. Without the flat-bottom potential, significant numbers of DIPC lipids are observed in the L_o domain and DPPC lipids are observed in the L_d domain. The interface fluctuates significantly as time evolves.

Please cite this article in press as: Kwon et al., Efficient calculation of the free energy for protein partitioning using restraining potentials, Biophysical Journal (2023), https://doi.org/10.1016/j.bpj.2022.07.031

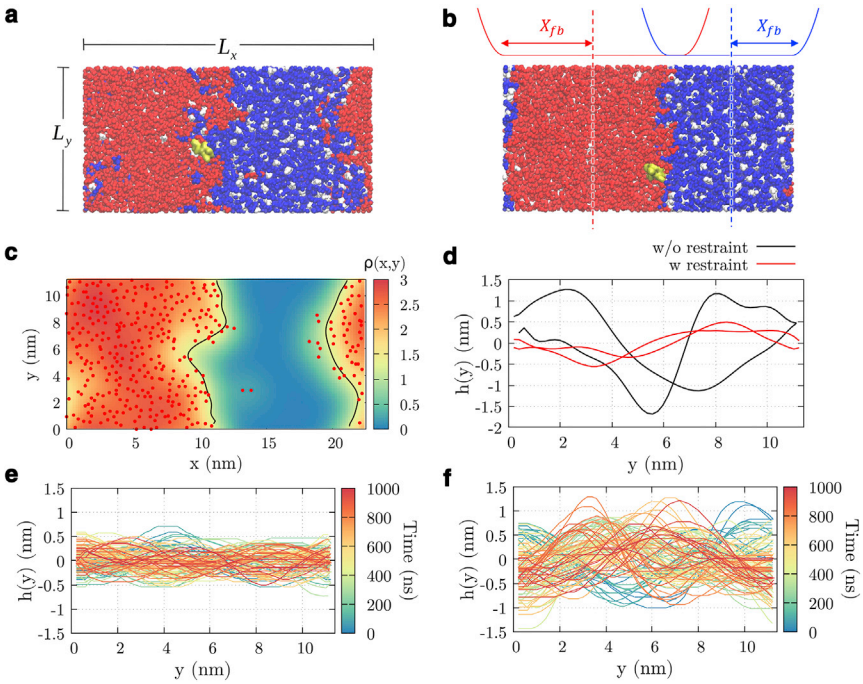

FIGURE 2 (*a* and *b*) Simulation snapshots of a lipid bilayer system composed of 900 lipids (*a*) without and (*b*) with a flat-bottom restraining potential. (*c*) The density field $\rho(x, y)$ derived from DIPC coordinates of (*a*). The two black lines represent the instantaneous interfaces. (*d*) The height of the interfacial fluctuations $h(y)$ in the phase-separated bilayer with and without the flat-bottom restraint with $\Delta = 5$ Å and 100 kJ mol^{-1} nm^{-2}. (*e*) and (*f*) show the change of a single interfacial line between $t = 0$ to 1 μs in the presence and absence of a restraining potential. To see this figure in color, go online.

This mixing is expected to impact packing at the very center of the L_d and L_o domains. The restraint potential prevents lipid mixing within domains, allowing for mixing to occur only in the neighborhood of the domain interfaces in the absence and presence of the restraining potential, respectively. The interfacial lines are constantly changing as time evolves, but fluctuations are limited to be within 1 nm, similar to the size of a lipid.

Characterization of the domain interface

In order to determine the instantaneous interface between the L_d and L_o domains, we employed the Willard-Chandler algorithm for identifying interfaces. We projected the coordinates of the D2A and D2B tail beads of the DIPC lipids (depicted as red dots in Fig. 2 *c*) onto the *xy* plane. A coarse-grained density field ρ was created based on the tail beads of DIPC (D2A and D2B):

$$\rho(\mathbf{r}, t) = \sum_i \varphi(|\mathbf{r} - \mathbf{r}_i(t)|), \tag{2}$$

where

$$\varphi(\mathbf{r}) = \frac{1}{2\pi\xi^2}\exp\left(-r^2 / 2\xi^2\right). \tag{3}$$

$\mathbf{r}_i(t)$ is the x and y coordinate of the ith particle at time t. The coarse-graining length ξ, defining the Gaussian width, was set to 1.2 nm. The interface at time t was defined as the set of points $\mathbf{s}$ where $\rho(\mathbf{s}, t) = 1.4$ nm^{-2}, which is the average value of the density field in the L_d and L_o domains. The density field was computed on a two-dimensional grid with a lattice spacing of 0.2 nm. $\varphi(\mathbf{r})$ was truncated and shifted to be zero at $r = 3\xi$. The interface was aligned along the y axis to minimize the line tension as $L_x \geq L_y$.

Calculation of interfacial line tension

Fluctuations of the domain interface were quantified in terms of the interfacial height fluctuation $h(y)$ (Fig. 2 *d*). The sum across the interface $\sum_i h(y_i)$ was set to 0 by definition. The line tension was determined using the power spectrum

$$H(k) = \frac{1}{L_y}\int_0^{L_y} dy h(y) e^{-iky}. \tag{4}$$

According to the capillary wave theory, the line tension λ is defined by the relation

$$\langle H(k)H(-k)\rangle = \langle |H(k)|^2\rangle = \frac{k_B T}{\lambda L_y k^2}, \tag{5}$$

where $k = 2\pi n/L_y$. We computed λ through the linear regression of $\langle |H(k)|^2\rangle$ versus k^{-2} using the first four wave modes with $n = 1$ to 4 corresponding to the four longest wavelengths.

We measured local fluctuations of the interface by dividing the interface into slabs of l nm and computed the root-mean-square fluctuations $\delta_h(l)$

$$\delta_h(l) = \frac{1}{L_y}\int_0^{L_y} \mathrm{d}y \left[\frac{1}{l}\int_y^{y+l} \mathrm{d}s \left(h(s) - h^-_{y,l}\right)^2\right], \tag{6}$$

where $h^-_{y,l}$ is the average of the interfacial height fluctuation h between y and $y + l$, i.e., $h_{y,l}{}^- = \frac{1}{l}\int_y^{y+l} \mathrm{d}s h(s)$. It shows how significant the interfacial fluctuations are within the length scale of l nm, for example, $\delta_h(l = 2nm)$ reports on averaged fluctuations of an interface of 2 nm length, and $\delta_h(l = L_y)$ is a measure of fluctuations across the full width of the system.

Please cite this article in press as: Kwon et al., Efficient calculation of the free energy for protein partitioning using restraining potentials, Biophysical Journal (2023), https://doi.org/10.1016/j.bpj.2022.07.031

Assessing lateral location and tail ordering of the lipids

The relative degree of ordering of lipid tails parallel to the bilayer normal was measured using the liquid crystal order parameter defined

$$P_2^k = \frac{1}{2}\langle 3\cos^2\theta_k - 1\rangle, \tag{7}$$

where θ_k is the angle between the tail vector of the kth lipids and the bilayer normal vector. The lipid tail vector extends from GL1 (GL2) to C2A (C2B) for DPPC and from GL1 (GL2) to D2A (D2B) for DIPC. Lipid tail groups were defined by C2A and C2B for DPPC, D2A and D2B for DIPC, and the centroid of R1, R2, R3, R4, and R5 for CHOL. Due to rapid flip flopping between leaflets, it was necessary to assign CHOL molecules to the upper or lower leaflet at each time frame. Each CHOL molecule was assigned to the upper (lower) leaflet if the distance between the head group of DPPC or DIPC (PO4 bead) in the upper (lower) leaflet and of CHOL (ROH bead) was within 1.5 nm.

The lateral packing of lipids was quantified by using the two-dimensional bond-orientational order parameters ψ_6 defined

$$\psi_6^k = \frac{1}{6}\sum_{l\in nn(k)}^{6} e^{i6\theta_{kl}}. \tag{8}$$

The coordinates of the kth tail particle and its six nearest neighbors ($l \in nn(k)$) were used to find a plane of best fit and then projected onto that plane. θ_{kl} is the angle between an arbitrary reference vector and a vector connecting k and l in the plane. The reference vector was chosen as the projection of a vector $\vec{r} = (1,0)$ onto the plane of best fit. The averaged bond orientational order parameter $|\psi_6|$ has a maximum value of 1 when the nearest neighbors present a perfect hexagonal packing.

In order to show how the lipid tail ordering and lateral packing change across the domain, P_2 and $|\psi_6|$ were calculated and plotted as a function of r_i, which is the distance of a lipid tail particle to the closest interfacial line on the xy plane. When a tail particle lies on the interface, r_i is equal to 0. r_i is negative (positive) value when a lipid is in the L_d (L_o) domain.

RESULTS

Lipid structure depends on system's aspect ratio

We assessed the tail ordering and lateral packing of lipids using P_2 and $|\psi_6|$ order parameters, respectively. Fig. 3 *a* and *c* depict the instantaneous P_2 and $|\psi_6|$ values of individual lipids in the smallest system having (L_x, L_y) = (22.4, 11.2 nm) not subject to the flat-bottom restraint at 295 K. P_2 and $|\psi_6|$ are shown as a function of r_i (Fig. 3 *b* and *d*), demonstrating how the bilayer structure changes on approaching the domain interface.

$P_2(r_i)$ converges to a constant value at large $|r_i|$, corresponding to the bulk domain. DIPC has $P_2 \approx 0.4$ in the L_d domain (negative r_i). DPPC has $P_2 \approx 0.9$, reflecting the high degree of ordering of lipids in the L_o domain (positive r_i). Near the interface, DIPC shows a higher tail ordering than observed in the L_d domain, and P_2 reaches up to 0.5. An increase in the population of neighboring DPPC lipids induces a modest degree of order in the DIPC lipid tails. Similarly, lipid molecules have a constant $|\psi_6|$ value at the domain center (see Fig. 3 *d*). Lipid packing as measured by P_2 and $|\psi_6|$ is observed to undergo significant changes

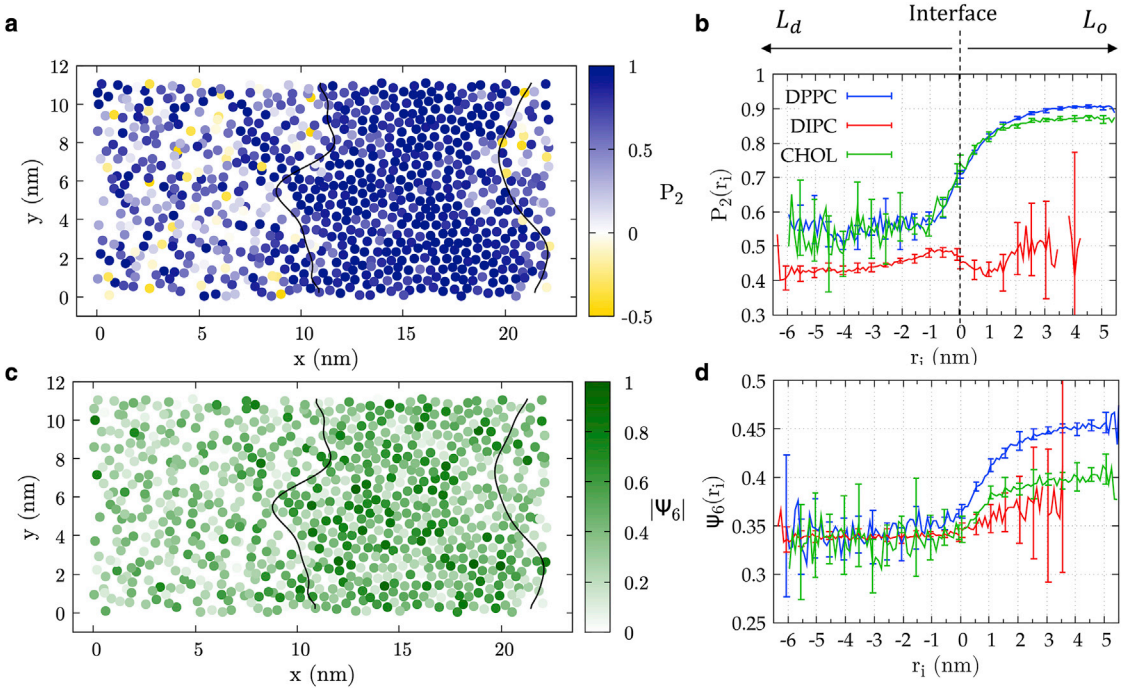

FIGURE 3 Characterization of the lipid structure and ordering across the interface in DPPC:DIPC:CHOL 40:40:20 bilayer at 295 K not subject to restraint. The size of system is $L_x = 22.4$ and $L_y = 11.2$ nm. (*a*) P_2 values of lipids for a representative snapshot are shown on the xy plane. (*b*) P_2 is plotted as a function of the distance from the interface r_i. (*c*) $|\psi_6|$ values of lipids for the same snapshot are shown on the xy plane. (*d*) $|\psi_6|$ is plotted as a function of the distance from the interface r_i. Error bars represent standard deviations. To see this figure in color, go online.

Please cite this article in press as: Kwon et al., Efficient calculation of the free energy for protein partitioning using restraining potentials, Biophysical Journal (2023), https://doi.org/10.1016/j.bpj.2022.07.031

specifically in the range -2 nm $< r_i <$ 3 nm (in terms of P_2) and -1 nm $< r_i <$ 3 nm (in terms of $|\psi_6|$). From those changes, we consider the interfacial region to be between 4 and 5 nm in width.

It is noticeable that lipid structures change up to a few nanometers from the interface. The area associated with the interface is substantial given that the interface itself has fluctuations on the order of a few nanometers. For the 2:1 x:y aspect ratio, we observed the interfacial height $h(y)$ to fluctuate around -2 to 1.5 nm (Fig. 2 *d*). We estimated the root-mean-square fluctuation $\delta_h = \sqrt{\langle h^2 \rangle}$, which depends on L_y, to be 0.90 nm for system size $L_x = 22.4$ and $L_y = 11.2$ nm. This implies that a substantially longer x axis is necessary to allow for lipid order representative of a bulk phase to manifest at the center of each lipid domain.

Fig. 4 depicts variations in bilayer structure with respect to system sizes in the x and y directions. Surprisingly, changing L_y had no impact on the tail ordering and lateral packing of DPPC. Fig. 4 *a* and *b* show the $P_2(r_i)$ and $|\psi_6|(r_i)$ profiles of DPPC with fixed L_x. The P_2 and $|\psi_6|$ profiles of DIPC and CHOL also show no change with respect to L_y (see Fig. S3).

In contrast, as shown in Fig. 4 *c* and *d*, changing L_x causes the P_2 of DPPC and DIPC to converge to different bulk values at different system sizes in the L_o and L_d domains, respectively. These observations confirm that DPPC becomes more ordered in the L_o domain and DIPC becomes more disordered in the L_d domain as the system's dimension perpendicular to the interface becomes larger.

Lateral packing of DPPC and CHOL in the L_o domain, measured in terms of $|\psi_6|$, is shown in Fig. 4 *e* and *f*. A higher degree of lateral ordering is observed for larger systems, but the impact on $|\psi_6|$ is less than observed for P_2. Similar values of P_2 and $|\psi_6|$ are measured for $L_x = 28.0$ and 33.6 nm in the bulk region, indicating convergence to bulk values for larger system sizes. The full range of the P_2 and $|\psi_6|$ profiles are presented in Fig. S4.

System size and aspect ratio can tune interfacial fluctuations

We measured the height of fluctuations in a local region of length l of the interface $\delta_h(l)$ (see Fig. 5). This quantity

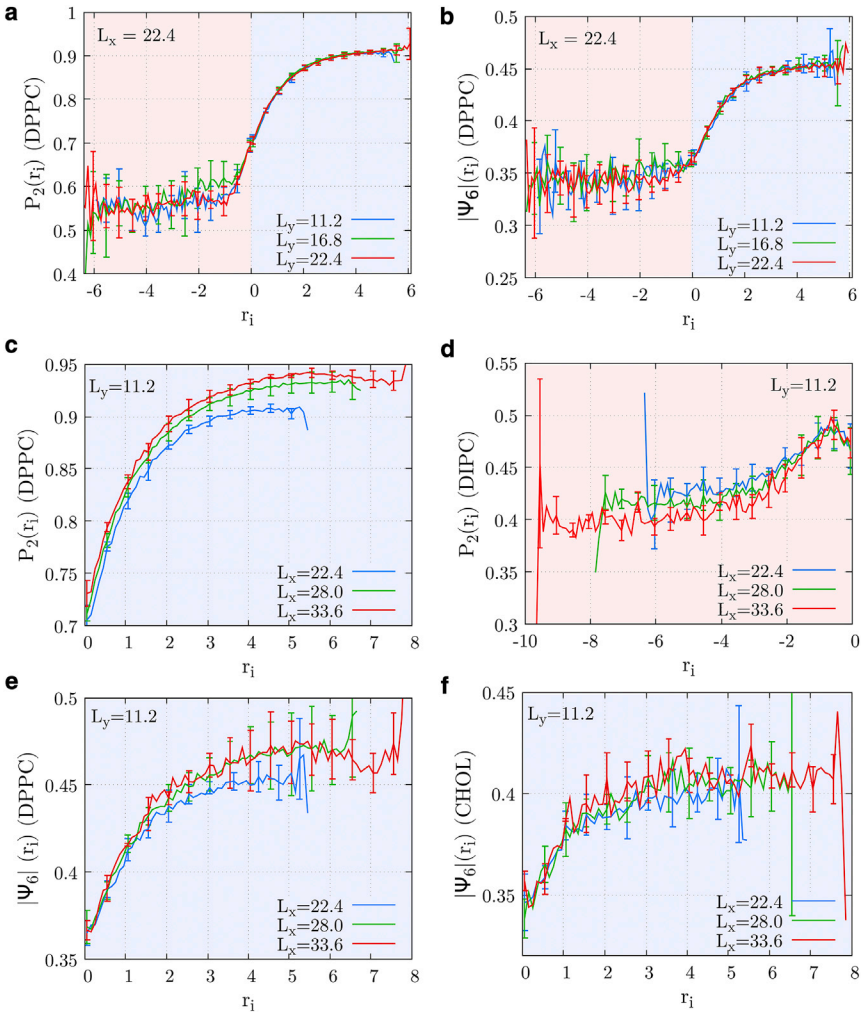

FIGURE 4 Lipid ordering is sensitive to changes in L_x but largely independent of changes in L_y. Structural order parameters are plotted as a function of the distance from the interface r_i for different systems sizes in simulations not subject to restraints. Red and blue region indicate the L_d and L_o domains. (*a* and *b*) Systems with fixed $L_x = 22.4$ nm (*a*) P_2 of DPPC, (*b*) $|\psi_6|$ of DPPC, and (*c*) P_2 of DPPC. (*c–f*) Systems with fixed $L_y = 11.2$ nm (*c*) P_2 of DPPC, (*d*) P_2 of DIPC, (*e*) $|\psi_6|$ of DPPC, and (*f*) $|\psi_6|$ of CHOL. To see this figure in color, go online.

Please cite this article in press as: Kwon et al., Efficient calculation of the free energy for protein partitioning using restraining potentials, Biophysical Journal (2023), https://doi.org/10.1016/j.bpj.2022.07.031

measures the average local fluctuations of the interface. When changing L_y with fixed $L_x = 22.4$ nm (Fig. 5 *a*), there is little change in the fluctuations for small l. The longest length-scale fluctuations are bounded by the length L_y. As such, systems with larger L_y support longer length-scale interfacial fluctuations.

On the other hand, when changing L_x with fixed $L_y = 11.2$ nm (Fig. 5 *b*), smaller fluctuations are observed at all length scales in large L_x systems. This indicates that the interfacial fluctuations are affected by the area of the bulk domain along the axis perpendicular to the interface. Similar to the P_2 and $|\psi_6|$ profiles in Fig. 4, the variation in the $\delta_h(l)$ curves with respect to L_x decreases as L_x increases, suggesting that the interfacial height eventually converges to the bulk value.

The trends in interfacial fluctuations at different length scales with respect to system sizes are not fully described by the line tension. Table 1 shows the line tension measured using capillary wave theory. The measured line tension increases with increasing L_y at constant L_x. Based on Fig. 5 *a*, it is expected that 1) short-range fluctuations are independent of L_y and 2) long-range fluctuations are suppressed in smaller L_y systems, consistent with a higher line tension. Since the capillary wave theory is based on only the four longest wavelength modes, estimating a line tension from the dependence of $\langle H(k)H(-k)\rangle$ on the wave mode k, the extent of the line fluctuations seen in $\delta_h(l)$ are not fully accounted for. λ is observed to increase with increasing L_x. As shown in Fig. 5 *b*, the fluctuations at all length scales decrease with increasing values of L_x.

PMF calculations at different system sizes

The PMF for the translation of the COM of trLAT between membrane domains was computed. At all system sizes, the minimum in the PMF was located at the interface. The vertical dashed lines in Fig. 6 *b* and *c* indicate the average location of the interfacial lines for each system. These results are consistent with our earlier observations (14) of the strong preference of trLAT to be localized at the interface (see Fig. 6 *a*). Given the free-energy bias of 4–8 k_BT for the interface, it is unlikely that trLAT would be observed in the L_o or L_d domains in unbiased MD simulations employing system sizes used in this study.

Fig. 6 *b* shows the PMF of two systems, at constant $L_x = 22.4$ nm and two values of $L_y = 11.2$ or 22.4 nm, in the absence of the interfacial flat-bottom restraint potential. We observe that trLAT is localized on the L_d side of the domain interface. We attribute this to enthalpically favorable lipid tail packing in the L_o domain that acts to exclude proteins, as observed previously in conventional MD simulation (6,12). The calculated PMF appears to be insensitive to variation in L_y. The lateral extent of trLAT in our simulation, measured by the radius of gyration in the xy plane, is about 1.1 nm. As such, the protein senses only short-range fluctuations on the length scale of a few nm. For those systems, the short-range fluctuations were observed to be the same regardless of L_y at fixed L_x (see Fig. 5). We observe that the minimum in the PMF varies greatly with system size L_x (see Fig. 6 *c*), with fluctuations in the interface being smaller in the larger L_x systems.

PMFs computed in systems not subject to the flat-bottom restraint do not manifest a plateau in free energy in the L_o region. The interfacial region over which P_2 and $|\psi_6|$ vary is as wide as 5 nm. In fact, it can be even wider, as the interface itself has fluctuations up to 1 nm. For the smallest system sizes ($L_x = 22.4$ and $L_y = 11.2$ nm), the width of the L_o domain is roughly 10 nm, leaving little bulk L_o domain. In addition, in the L_o domain, the protein makes strong contact with DIPC. Due to the high degree of lateral packing in the L_o domain, the DIPC lipids and protein have significant interaction. Large fluctuations of the interface in restraint-free systems allow the protein near the interface to contact DIPC, driving the formation of a distorted interfacial region as depicted in Fig. 8 *a*. The substantial increase in free energy as the protein is translated into the L_o domains is consistent with observations from prior simulation studies (7,14,26–28).

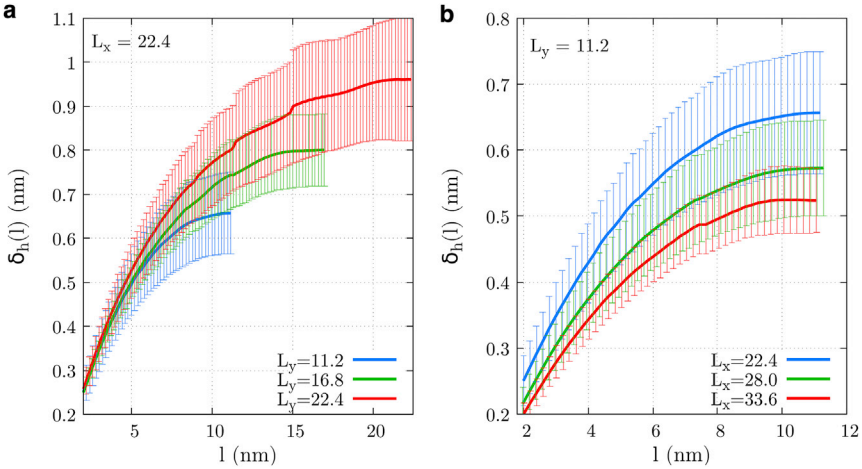

FIGURE 5 (*a* and *b*) The root-mean-square fluctuations $\delta_h(l)$ as a function of l for varying (*a*) L_x and (*b*) L_y. Interfacial fluctuations at all length scales are impacted by a change in L_x and the width of the interface. Error bars represent standard deviations. To see this figure in color, go online.

Please cite this article in press as: Kwon et al., Efficient calculation of the free energy for protein partitioning using restraining potentials, Biophysical Journal (2023), https://doi.org/10.1016/j.bpj.2022.07.031

TABLE 1 The line tension λ measured using capillary wave theory

L_x (nm)		22.4			28.0			33.6	
L_y (nm)	11.2	16.8	22.4	11.2	16.8	22.4	11.2	16.8	22.4
λ (pN/nm)	6.1 ± 1.7	7.8 ± 2.1	8.0 ± 2.8	8.3 ± 3.0	8.8 ± 2.3	12.1 ± 6.4	9.0 ± 1.9	11.6 ± 2.9	18.4 ± 6.0

By employing a flat-bottom restraint, we can significantly reduce the interfacial fluctuations and modulate lipid structure near the interface as well as in bulk domains. Fig. 7 shows the bilayer structure and interfacial fluctuations for a small system with $L_x = 22.4$ nm (900 lipids) and a large system with $L_x = 28.0$ nm (1350 lipids). In the absence of restraints, the bulk P_2 value was diminished in the small system. However, by employing restraints, we can induce higher lipid tail ordering in the small system, making the measured bulk P_2 value close to that of the large system. Considering variations in P_2 and $|\psi_6|$, we conclude that the smaller system with a flat-bottom restraint shows good agreement with the large system.

By imposing the potential restraint, the interfacial fluctuation is significantly suppressed, and interfacial line fluctuations become less sensitive to L_x (see Fig. 7 *c*). The use of the flat-bottom restraint also prevents distortions of the interface due to protein-DIPC contacts in the L_o domain (see Fig. 8 *b*). The small fluctuations at the interface stabilized by the flat-bottom restraint allow the bilayer to manifest bulk domains. In addition, the restraint potential aligns the interface and makes the interfacial region more uniform. As such, we observe that the PMF reaches a plateau, in both the L_d and L_o domains, when applying the flat-bottom restraint (see Fig. 8 *c*). The minimum in the PMF is observed to decrease as L_x is increased, with the minimum in the PMF being similar to that observed in the large system.

DISCUSSION

At macroscopic length scales, the partition coefficients of proteins will be determined by the free-energy difference associated with moving protein between bulk domains. In experiments, partitioning is assessed by measuring the relative population of protein tagged with a fluorescent marker in phase-separated model membrane systems (9–11). In GUV experiments, trLAT is observed to be partitioned into the L_d domain (41). In MD simulation studies, proteins tend to accumulate at the L_o-L_d interface. The finite size of the simulation system contributes to this discrepancy because the ratio of the interfacial length to the bulk area is artificially large in conventional MD simulations. Given that the length scale of lipid raft domains ranges broadly from a few to several hundred nanometers (42–46), it is important to consider how finite system size impacts a protein's partitioning.

We hypothesize a three-state model for the PMF by dividing the system into three regimes: L_o domain, L_d domain, and the interface (see Fig. 9 *a*). The simulation data for the PMF (red squares) is extended toward the bulk (black solid lines), allowing us to postulate the thermodynamic limit of the PMF computed in MD simulations. The PMF is expanded from $x = -L$ to L, where $2L$ is the hypothetical system size along the x axis. The interface is in between x_d and x_o, and $x = 0$ is the average

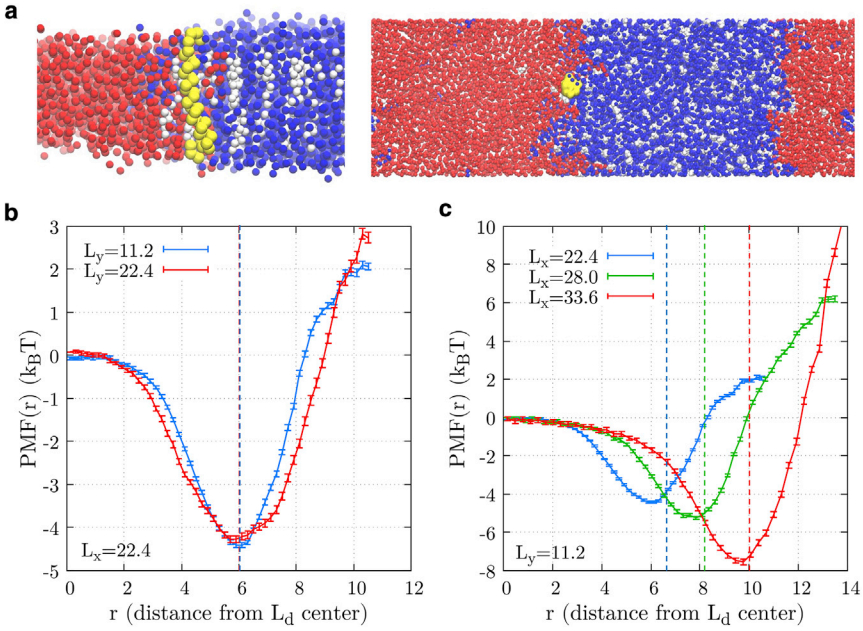

FIGURE 6 (*a*) Simulation snapshots of trLAT (*yellow*) located at the domain boundary. DPPC, DIPC, and CHOL are represented as blue, red, and white beads. (*b* and *c*) The PMFs obtained from umbrella sampling simulations are plotted for different (*b*) L_y and (*c*) L_x. Both the position and depth of the minimum are sensitive to changes in L_x and the interfacial width. To see this figure in color, go online.

Please cite this article in press as: Kwon et al., Efficient calculation of the free energy for protein partitioning using restraining potentials, Biophysical Journal (2023), https://doi.org/10.1016/j.bpj.2022.07.031

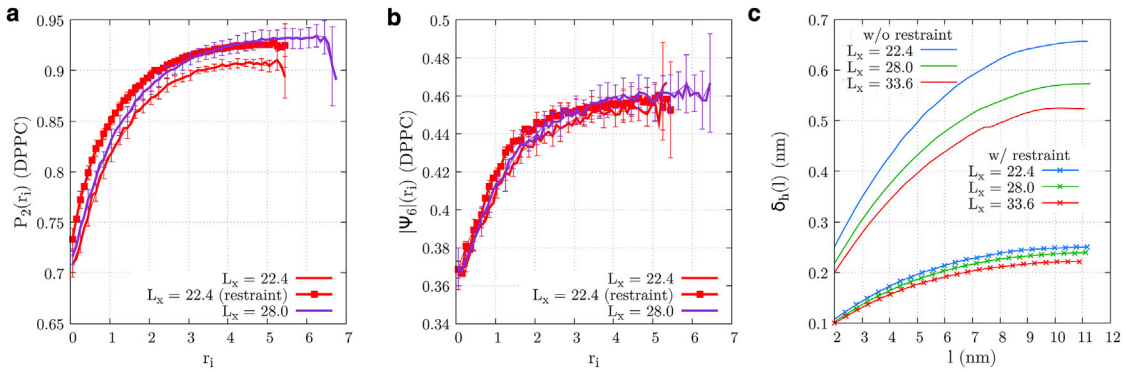

FIGURE 7 (*a* and *b*) P_2 (*a*) and $|\psi_6|$ (*b*) profiles for DPPC lipids in phase-separated ternary lipid bilayers with and without the restraint potential. (*c*) The interfacial height fluctuation $\delta_h(l)$ is plotted for bilayers with and without the flat-bottom restraint potential. Fluctuations in the presence of the restraint are reduced and largely independent of L_x and interfacial width. To see this figure in color, go online.

position of the interface in simulations. The red dashed box in Fig. 9 *a* extends over half of the system size of the simulation.

Fig. 9 *b* and *c* show the length of the interface ($l_{interface}$) and the free-energy difference between the L_d and L_o domains (ΔW_{do}) from the extended PMF computed at different system sizes L_x and in the presence of the restraint. $l_{interface}$ and ΔW_{do} extracted from the hypothesized macroscopic PMF vary significantly with system size.

This is an artifact of the finite size of the system that manifests significant fluctuations compared with the overall system size. As discussed in Fig. 8, the system in the absence of the restraint potential exhibits a continuous increase of free energy in the L_o domain due to enhanced lipid packing and substantial distortion of the interface. As such, $l_{interface}$ reaches up to values comparable to half of the system sizes L_x, implying that the true bulk region of each domain hardly appears in the simulations. On the other hand, $l_{interface}$ of the restrained membrane system of $L_x = 22.4$ nm is approximately half that of the system of the same size in the absence of the restraint. This reduces the artifact that arose from the system size dependence and leads to values of ΔW_{do} that are not affected by the interface distortion. The distorted interface and displaced lipids do not readily relax within the simulation timescale. As such, the energy penalty associated with the interfacial distortion accumulates as the protein moves toward the center of the L_o domain. This results in an abnormal increase in ΔW_{do}, apparent in the asymptotic value of the PMF. This emphasizes how the use of the restraining potentials acts to stabilize the bulk L_o region, in small systems, and prevent nonequilibrium distortion of the interface in large systems.

The discrepancy between partitioning in MD simulations and GUVs was previously suggested to occur due to the saturation of the interface with proteins at high concentrations (6). In this work, we add additional detail to this theory by characterizing the thermodynamic equilibrium of protein partitioning using a three-state model with varying system sizes. In the three-state model analysis, we employed the PMF of the system having $L_x = 22.4$ and $L_y = 11.2$ nm in the presence of restraints. We further assumed that PMF remains unchanged regardless of the increase of protein concentration in the membrane.

Most prior simulation studies of protein partitioning have evaluated the PMF for a single protein moving between domains across an interface. A minimum in the free energy is typically observed to be located at the interface. For smaller systems sizes, such as those commonly employed in MD simulations, the areas of the bulk domains are small, and the probability of observing the protein at the interface is

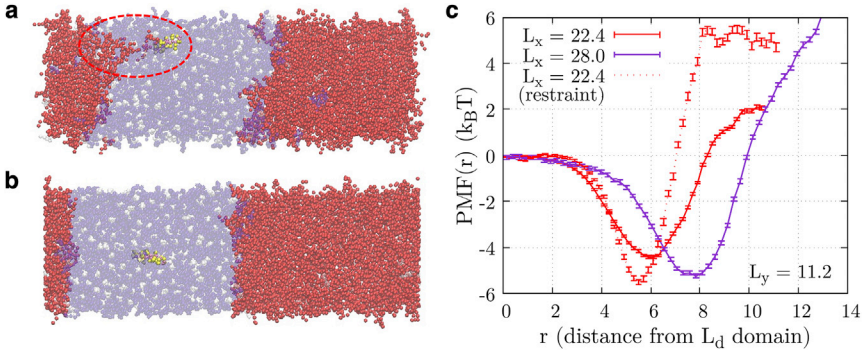

FIGURE 8 (*a* and *b*) Snapshots from the umbrella sampling simulation of ternary phase-separated lipid bilayers with $L_x = 33.6$ and $L_y = 11.2$ nm both (*a*) without and (*b*) with the flat-bottom restraint potential. In the dashed region, we observe a strong interaction between protein and DIPC lipid molecules. (*c*) The computed PMF is shown with and without the flat-bottom restraint potential. The position of the minimum in the PMF is largely independent of the restraint, while the depth of the minimum is consistent with that observed in the large systems. To see this figure in color, go online.

Please cite this article in press as: Kwon et al., Efficient calculation of the free energy for protein partitioning using restraining potentials, Biophysical Journal (2023), https://doi.org/10.1016/j.bpj.2022.07.031

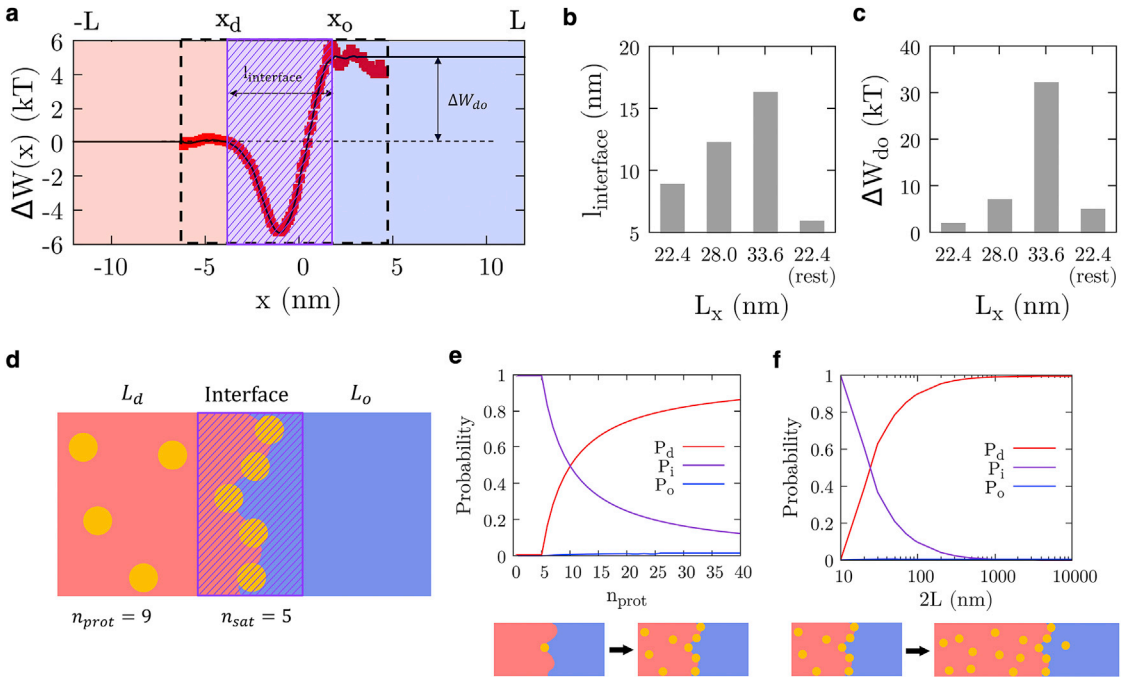

FIGURE 9 (*a*) Extended PMF curves for the three-state model in our smallest system $L_x = 22.4$ and $L_y = 11.2$ nm without the restraint. Red squares are simulation data, and black solid lines indicate the hypothesized PMF expanded toward $-L$ to L. Red, blue, and purple indicate the L_d, L_o, and the interface, respectively. (*b* and *c*) The length of the interface ($l_{interface}$) (*b*) and the free-energy difference (ΔW_{do}) (*c*) for different simulations are shown. (*d*) A schematic of protein partitioning in the three-state model is shown. Yellow disks represent proteins. Of the total number n_{prot} proteins, n_{sat} proteins saturate the interface, while the remainder are partitioned to either the L_d or L_o domains. (*e* and *f*) The probability of each state (L_d, L_o, and the interface) is shown for which (*e*) the total number of proteins n_{prot} changes with fixed $n_{sat} = 5$ and $2L = 22.4$ nm and (*f*) the system size $2L$ changes with fixed $n_{sat}= 5$ and protein number density $n_{prot}/2L = 0.4$ nm^{-1}. To see this figure in color, go online.

high. However, as the area of the bulk domains grows, the probability of a protein being observed at the interface diminishes. In the thermodynamic limit, as the bulk domains scale as the square of the system size, while the interface scales linearly with system size, the probability of observing the protein at the interface becomes negligible compared with the bulk domains. Fig. 9 *d* shows a schematic figure of the model where n_{prot} is the total number of proteins and n_{sat} is the maximum number of proteins at the interface saturating the interface. The probability of each state for a single protein was computed as

$$\begin{aligned} p_d &= \frac{1}{Z}\int_{-L}^{x_d} e^{-\Delta W(x)/kT}\mathrm{d}x \\ p_i &= \frac{1}{Z}\int_{x_d}^{x_o} e^{-\Delta W(x)/kT}\mathrm{d}x \\ p_o &= \frac{1}{Z}\int_{x_o}^{L} e^{-\Delta W(x)/kT}\mathrm{d}x \\ Z &= \int_{-L}^{L} e^{-\Delta W(x)/kT}\mathrm{d}x \end{aligned} \quad . \tag{9}$$

We calculated the probability p^j of d, i, and o states for a protein j. We limit the maximum number of proteins at the interface (n_{sat}) so that $(n_{prot} - n_{sat})$ proteins can be partitioned between the L_o and L_d domains. The partitioning probability of proteins are calculated as the average over total n_{prot} proteins, i.e., $P_d = \langle p_d^j \rangle$, $P_i = \langle p_i^j \rangle$, and $P_o = \langle p_o^j \rangle$.

Fig. 9 *e* shows how the probabilities change with respect to the total number of proteins in the membrane. As the system size is fixed to $2L = 22.4$ nm, which is equivalent to that of the original MD simulation, increasing n_{prot} increases the protein concentration of the system. Given that the lateral radius of gyration of trLAT is $2R_g \approx 2.2$ nm and L_y (the axis parallel to the interface) is 11.2 nm, we take $n_{sat} = 5$. When the total number of proteins is less than n_{sat}, all proteins are observed to be located at the interface $(P_i \approx 1)$, as the protein is stabilized most at the interface. P_d and P_o increase once n_{prot} exceeds n_{sat}. For the case of 1800 lipids in the system of $L_x = 22.4$ and $L_y = 11.2$ nm, $n_{prot} = 9$ corresponds to the protein/lipid ratio 1/200, which is frequently used in experiments. P_i and P_d become comparable at this point even in a system size that is small compared with GUVs employed in experiments, which are on the order of tens of μm. The probability at the interface decreases rapidly as the protein concentration increases.

The high interface/bulk ratio of the simulations also contributes to the observed discrepancy of protein partitioning in experiments and simulations. The ratio of the interface

Please cite this article in press as: Kwon et al., Efficient calculation of the free energy for protein partitioning using restraining potentials, Biophysical Journal (2023), https://doi.org/10.1016/j.bpj.2022.07.031

to the bulk area for lipid bilayer simulations with a box dimension L would be O (L/L^2), and for GUV of a radius r, there is similar scaling as O (r/r^2). Fig. 9 *f* shows how the probabilities change with the system size $2L$. The total number density of protein was held constant to mimic the experimental conditions of a 1:200 protein:lipid ratio. We postulate that the system expands in the x dimension only, thus n_{prot} scaled linearly with L, such that $n_{prot}/2L \approx 0.4$ molecule/nm. The probability at the interface P_i becomes effectively zero at $2L > 1$ μm despite the large free-energy difference of -5 kT between the interface and the L_d domain. These results demonstrate that while we expect to see saturation of the interfacial region with proteins in smaller system sizes, the relative population of protein at the interface diminishes with increasing system size as more protein enters the bulk regions, establishing the equilibrium partition coefficient of protein between the L_o and L_d domains. These results of the three-state model provide an explanation for the seemingly inconsistent partitioning tendency in experiments and simulations. Even if proteins prefer the interface at the single-molecule level, the larger number of proteins causes saturation of the interface, thereby the preferential partitioning to the interface is underestimated in experiments.

CONCLUSION

The preferential partitioning of TM proteins between distinct lipid domains in phase-separated membranes has been conjectured to play a critical role in a variety of fundamental biophysical processes, including facilitating cell signaling, enabling concerted enzymatic reactions, and facilitating protein assembly and amyloid aggregation. While simple rules related to hydrophobic mismatch capture some elements of preferential protein partitioning, predictions are often at odds with experiments. Detailed simulations of protein partitioning, from which one may compute the PMF and partition coefficients for the translation of proteins between domains, have proved challenging for two reasons. System sizes required for the simulation of stable phase-separated states are prohibitively large. In addition, the sizes of fluctuations of the protein interface, on the scale of the proteins themselves, make it difficult to clearly define the interfacial region and the separate L_o and L_d domains. As such, to date, it has not been possible to quantitatively predict equilibrium partition coefficients and the underlying free energies using computer simulation.

In this work, we have explored methods for the efficient simulation of phase-separated lipid bilayers for the purpose of computing free-energy differences for the partitioning of TM proteins between distinct membrane domains. We exploit the use of flat-bottom potential energy functions to create stable phase-separated states for small lipid numbers and rectangular aspect ratios, which reduce the interfacial length and thereby enhance the stability of the phase-separated states. A thorough evaluation of the lipid structure, in terms of tail order and headgroup packing, allows us to assess the impact of the imposed restraints on the state of the bilayer. We demonstrate that in the presence of appropriate restraints, small system sizes can display stable phase-separated states with interfacial fluctuations and bulk domain structures consistent with those of larger systems in the absence of restraints. As such, the proposed methodology can be used to address the current need to compute free energies of protein partitioning and associated partition coefficients. This opens the door for studies designed to critically examine the conjectured role of preferential partitioning of proteins to membrane domains in supporting membrane protein functions.

SUPPORTING MATERIAL

Supporting material can be found online at https://doi.org/10.1016/j.bpj.2022.07.031.

AUTHOR CONTRIBUTIONS

S.K., G.A.P., and J.E.S. designed the research; S.K. performed the research and analyzed the data; S.K., G.A.P., and J.E.S. wrote the manuscript.

ACKNOWLEDGMENTS

The authors gratefully acknowledge the generous support of the National Science Foundation (grant no. CHE-1900416), the National Institutes of Health (grant no. R01 GM107703), and the high performance computing resources of the Boston University Shared Computing Cluster (SCC). We thank Conor Abraham and Ayan Majumder for helpful discussions.

DECLARATION OF INTERESTS

The authors declare no competing interests.

REFERENCES

1. Simons, K., and J. L. Sampaio. 2011. Membrane organization and lipid rafts. *Cold Spring Harb. Perspect. Biol.* 3:a004697.
2. Sengupta, P., B. Baird, and D. Holowka. 2007. Lipid rafts, fluid/fluid phase separation, and their relevance to plasma membrane structure and function. *Semin. Cell Dev. Biol.* 18:583–590.
3. Staubach, S., and F. G. Hanisch. 2011. Lipid rafts: signaling and sorting platforms of cells and their roles in cancer. *Exp. Rev. Proteonomics.* 8:263–277.
4. Taylor, D. R., and N. M. Hooper. 2007. Role of lipid rafts in the processing of the pathogenic prion and Alzheimer's amyloid-β proteins. *Semin. Cell Dev. Biol.* 18:638–648.
5. Diaz-Rohrer, B., K. R. Levental, and I. Levental. 2014. Rafting through traffic: membrane domains in cellular logistics. *Biochim. Biophys. Acta Biomembr.* 1838:3003–3013.
6. Lin, X., A. A. Gorfe, and I. Levental. 2018. Protein partitioning into ordered membrane domains: insights from simulations. *Biophys. J.* 114:1936–1944.

7. Janosi, L., Z. Li, …, A. A. Gorfe. 2012. Organization, dynamics, and segregation of Ras nanoclusters in membrane domains. *Proc. Natl. Acad. Sci. USA.* 109:8097–8102.
8. Lin, X., and A. A. Gorfe. 2019. Understanding membrane domain-partitioning thermodynamics of transmembrane domains with potential of mean force calculations. *J. Phys. Chem. B.* 123:1009–1016.
9. Lorent, J. H., B. Diaz-Rohrer, …, I. Levental. 2017. Structural determinants and functional consequences of protein affinity for membrane rafts. *Nat. Commun.* 8:1219.
10. Capone, R., A. Tiwari, …, A. K. Kenworthy. 2021. The C99 domain of the amyloid precursor protein resides in the disordered membrane phase. *J. Biol. Chem.* 296:100652.
11. Sezgin, E., I. Levental, …, P. Schwille. 2012. Partitioning, diffusion, and ligand binding of raft lipid analogs in model and cellular plasma membranes. *Biochim. Biophys. Acta Biomembr.* 1818:1777–1784.
12. Schafer, L. V., D. H. de Jong, …, S. J. Marrink. 2011. Lipid packing drives the segregation of transmembrane helices into disordered lipid domains in model membranes. *Proc. Natl. Acad. Sci. USA.* 108:1343–1348.
13. Nikolaus, J., S. Scolari, …, A. Herrmann. 2010. Hemagglutinin of influenza virus partitions into the nonraft domain of model membranes. *Biophys. J.* 99:489–498.
14. Bandara, A., A. Panahi, …, J. E. Straub. 2019. Exploring the impact of proteins on the line tension of a phase-separating ternary lipid mixture. *J. Chem. Phys.* 150:204702.
15. Park, S., M. S. Yeom, …, W. Im. 2019. Quantitative characterization of protein–lipid interactions by free energy simulation between binary bilayers. *J. Chem. Theor. Comput.* 15:6491–6503.
16. Marsh, D. 2009. Cholesterol-induced fluid membrane domains: a compendium of lipid-raft ternary phase diagrams. *Biochim. Biophys. Acta Biomembr.* 1788:2114–2123.
17. Pantelopulos, G. A., and J. E. Straub. 2018. Regimes of complex lipid bilayer phases induced by cholesterol concentration in MD simulation. *Biophys. J.* 115:2167–2178.
18. Feigenson, G. W. 2007. Phase boundaries and biological membranes. *Annu. Rev. Biophys. Biomol. Struct.* 36:63–77.
19. Ackerman, D. G., and G. W. Feigenson. 2015. Multiscale modeling of four-component lipid mixtures: domain composition, size, alignment, and properties of the phase interface. *J. Phys. Chem. B.* 119:4240–4250.
20. Pantelopulos, G. A., T. Nagai, …, J. E. Straub. 2017. Critical size dependence of domain formation observed in coarse-grained simulations of bilayers composed of ternary lipid mixtures. *J. Chem. Phys.* 147:095101.
21. Carpenter, T. S., C. A. López, …, S. Gnanakaran. 2018. Capturing phase behavior of ternary lipid mixtures with a refined martini coarse-grained force field. *J. Chem. Theor. Comput.* 14:6050–6062.
22. Holcomb, C. D., P. Clancy, and J. A. Zollweg. 1993. A critical study of the simulation of the liquid-vapour interface of a Lennard-Jones fluid. *Mol. Phys.* 78:437–459.
23. Chen, L. J. 1995. Area dependence of the surface tension of a Lennard-Jones fluid from molecular dynamics simulations. *J. Chem. Phys.* 103:10214–10216.
24. Orea, P., J. López-Lemus, and J. Alejandre. 2005. Oscillatory surface tension due to finite-size effects. *J. Chem. Phys.* 123:114702.
25. Nilsson, D., and A. Irbäck. 2021. Finite-size shifts in simulated protein droplet phase diagrams. *J. Chem. Phys.* 154:235101.
26. Risselada, H. J., and S. J. Marrink. 2008. The molecular face of lipid rafts in model membranes. *Proc. Natl. Acad. Sci. USA.* 105:17367–17372.
27. Domański, J., S. J. Marrink, and L. V. Schäfer. 2012. Transmembrane helices can induce domain formation in crowded model membranes. *Biochim. Biophys. Acta Biomembr.* 1818:984–994.
28. Rosetti, C. M., G. G. Montich, and C. Pastorino. 2017. Molecular insight into the line tension of bilayer membranes containing hybrid polyunsaturated lipids. *J. Phys. Chem. B.* 121:1587–1600.
29. Marrink, S. J., H. J. Risselada, …, A. H. de Vries. 2007. The MARTINI force field: coarse grained model for biomolecular simulations. *J. Phys. Chem. B.* 111:7812–7824.
30. Melo, M. N., H. I. Ingólfsson, and S. J. Marrink. 2015. Parameters for Martini sterols and hopanoids based on a virtual-site description. *J. Chem. Phys.* 143:243152.
31. Pronk, S., S. Páll, …, E. Lindahl. 2013. GROMACS 4.5: a high-throughput and highly parallel open source molecular simulation toolkit. *Bioinformatics.* 29:845–854.
32. Abraham, M. J., T. Murtola, …, E. Lindahl. 2015. GROMACS: high performance molecular simulations through multi-level parallelism from laptops to supercomputers. *SoftwareX.* 1-2:19–25.
33. Wassenaar, T. A., H. I. Ingólfsson, …, S. J. Marrink. 2015. Computational lipidomics with insane : a versatile tool for generating custom membranes for molecular simulations. *J. Chem. Theor. Comput.* 11:2144–2155.
34. Bussi, G., and M. Parrinello. 2007. Accurate sampling using Langevin dynamics. *Phys. Rev. E Stat. Nonlin. Soft Matter Phys.* 75:1–7.
35. Berendsen, H. J., J. P. Postma, …, J. R. Haak. 1984. Molecular dynamics with coupling to an external bath. *J. Chem. Phys.* 81:3684–3690.
36. de Jong, D. H., S. Baoukina, …, S. J. Marrink. 2016. Martini straight: boosting performance using a shorter cutoff and GPUs. *Comput. Phys. Commun.* 199:1–7.
37. Grossfield, A.. WHAM: The Weighted Histogram Analysis Method. version 2.0.11. http://membrane.urmc.rochester.edu/wordpress/?page_id=126.
38. Kumar, S., D. Bouzida, …, J. M. Rosenberg. 1992. The weighted histogram analysis method for free-energy calculations on biomolecules. I. The method. *J. Comput. Chem.* 13:1011–1021.
39. Ingólfsson, H. I., M. N. Melo, …, S. J. Marrink. 2014. Lipid organization of the plasma membrane. *J. Am. Chem. Soc.* 136:14554–14559.
40. Vögele, M., J. Köfinger, and G. Hummer. 2018. Hydrodynamics of diffusion in lipid membrane simulations. *Phys. Rev. Lett.* 120:268104.
41. Shogomori, H., A. T. Hammond, …, D. A. Brown. 2005. Palmitoylation and intracellular domain interactions both contribute to raft targeting of linker for activation of T cells. *J. Biol. Chem.* 280:18931–18942.
42. Ratajczak, M. Z., and M. Adamiak. 2015. Membrane lipid rafts, master regulators of hematopoietic stem cell retention in bone marrow and their trafficking. *Leukemia.* 29:1452–1457.
43. Ilya Levental, M. G., and K. Simons. 2011. Raft domains of variable properties and compositions in plasma membrane vesicles. *Proc. Natl. Acad. Sci. USA.* 108:11411–11416.
44. Pralle, A., P. Keller, …, J. Hörber. 2000. Sphingolipid–cholesterol rafts diffuse as small entities in the plasma membrane of mammalian cells. *J. Cell Biol.* 148:997–1008.
45. Eggeling, C., C. Ringemann, …, S. W. Hell. 2009. Direct observation of the nanoscale dynamics of membrane lipids in a living cell. *Nature.* 457:1159–1162.
46. Schütz, G. J., G. Kada, …, H. Schindler. 2000. Properties of lipid microdomains in a muscle cell membrane visualized by single molecule microscopy. *EMBO J.* 19:892–901.